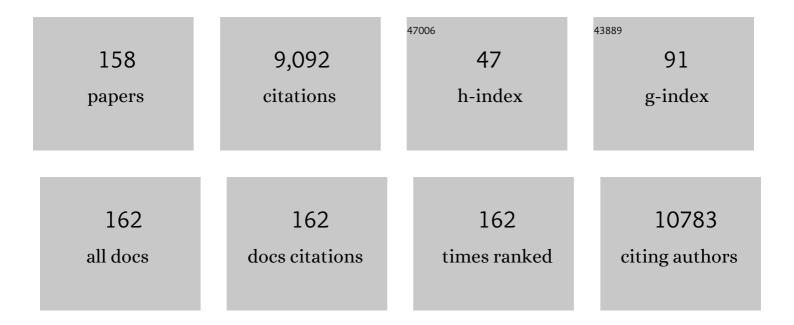
Antonio Lanzirotti

List of Publications by Year in descending order

Source: https://exaly.com/author-pdf/6031222/publications.pdf Version: 2024-02-01



#	Article	IF	CITATIONS
1	Comet 81P/Wild 2 Under a Microscope. Science, 2006, 314, 1711-1716.	12.6	848
2	Localization of Iron in Arabidopsis Seed Requires the Vacuolar Membrane Transporter VIT1. Science, 2006, 314, 1295-1298.	12.6	614
3	Mineralogy and Petrology of Comet 81P/Wild 2 Nucleus Samples. Science, 2006, 314, 1735-1739.	12.6	589
4	Synchrotron-based infrared and X-ray imaging shows focalized accumulation of Cu and Zn co-localized with β-amyloid deposits in Alzheimer's disease. Journal of Structural Biology, 2006, 155, 30-37.	2.8	521
5	TitaniQ under pressure: the effect of pressure and temperature on the solubility of Ti in quartz. Contributions To Mineralogy and Petrology, 2010, 160, 743-759.	3.1	388
6	Elemental Compositions of Comet 81P/Wild 2 Samples Collected by Stardust. Science, 2006, 314, 1731-1735.	12.6	200
7	High-precision determination of iron oxidation state in silicate glasses using XANES. Chemical Geology, 2009, 268, 167-179.	3.3	183
8	Coprecipitation of Uranium(VI) with Calcite: XAFS, micro-XAS, and luminescence characterization. Geochimica Et Cosmochimica Acta, 2001, 65, 3491-3503.	3.9	180
9	Phloem transport of arsenic species from flag leaf to grain during grain filling. New Phytologist, 2011, 192, 87-98.	7.3	170
10	lce-VII inclusions in diamonds: Evidence for aqueous fluid in Earth's deep mantle. Science, 2018, 359, 1136-1139.	12.6	166
11	Successful Reproduction Requires the Function of Arabidopsis YELLOW STRIPE-LIKE1 and YELLOW STRIPE-LIKE3 Metal-Nicotianamine Transporters in Both Vegetative and Reproductive Structures. Plant Physiology, 2010, 154, 197-210.	4.8	164
12	Metal Speciation and Its Role in Bioaccessibility and Bioavailability. Reviews in Mineralogy and Geochemistry, 2006, 64, 59-113.	4.8	158
13	Arsenic Speciation and Reactivity in Poultry Litter. Environmental Science & Technology, 2003, 37, 4083-4090.	10.0	139
14	Increased brain iron coincides with early plaque formation in a mouse model of Alzheimer's disease. NeuroImage, 2011, 55, 32-38.	4.2	123
15	High concentration of zinc in sub-retinal pigment epithelial deposits. Experimental Eye Research, 2007, 84, 772-780.	2.6	117
16	Amyloid plaques in PSAPP mice bind less metal than plaques in human Alzheimer's disease. NeuroImage, 2009, 47, 1215-1220.	4.2	117
17	Yttrium zoning in metamorphic garnets. Geochimica Et Cosmochimica Acta, 1995, 59, 4105-4110.	3.9	112
18	Using synchrotron X-ray fluorescence microprobes in the study of metal homeostasis in plants. Annals of Botany, 2009, 103, 665-672.	2.9	109

#	Article	IF	CITATIONS
19	Evidence That the ZNT3 Protein Controls the Total Amount of Elemental Zinc in Synaptic Vesicles. Journal of Histochemistry and Cytochemistry, 2008, 56, 3-6.	2.5	108
20	THE SPECIATION OF ARSENIC IN IRON OXIDES IN MINE WASTES FROM THE GIANT GOLD MINE, N.W.T.: APPLICATION OF SYNCHROTRON MICRO-XRD AND MICRO-XANES AT THE GRAIN SCALE. Canadian Mineralogist, 2005, 43, 1205-1224.	1.0	106
21	Subretinal Pigment Epithelial Deposition of Drusen Components Including Hydroxyapatite in a Primary Cell Culture Model. , 2017, 58, 708.		105
22	ARSENIC MINERALOGY OF NEAR-SURFACE TAILINGS AND SOILS: INFLUENCES ON ARSENIC MOBILITY AND BIOACCESSIBILITY IN THE NOVA SCOTIA GOLD MINING DISTRICTS. Canadian Mineralogist, 2009, 47, 533-556.	1.0	101
23	Identification of hydroxyapatite spherules provides new insight into subretinal pigment epithelial deposit formation in the aging eye. Proceedings of the National Academy of Sciences of the United States of America, 2015, 112, 1565-1570.	7.1	101
24	Abiotic Reductive Immobilization of U(VI) by Biogenic Mackinawite. Environmental Science & Technology, 2013, 47, 2361-2369.	10.0	100
25	Speciation Matters: Bioavailability of Silver and Silver Sulfide Nanoparticles to Alfalfa (<i>Medicago) Tj ETQq1 1 0</i>	.784314 r 10.0	gBT /Overloc 96
26	Spatial Distribution and Speciation of Lead around Corroding Bullets in a Shooting Range Soil Studied by Micro-X-ray Fluorescence and Absorption Spectroscopy. Environmental Science & Technology, 2005, 39, 4808-4815.	10.0	90
27	Geochronology and geochemistry of multiple generations of monazite from the Wepawaug Schist, Connecticut, USA: implications for monazite stability in metamorphic rocks. Contributions To Mineralogy and Petrology, 1996, 125, 332-340.	3.1	88
28	In Situ Reduction of Chromium(VI) in Heavily Contaminated Soils through Organic Carbon Amendment. Journal of Environmental Quality, 2003, 32, 1641-1649.	2.0	81
29	Emissions and encapsulation of cadmium in CdTe PV modules during fires. Progress in Photovoltaics: Research and Applications, 2005, 13, 713-723.	8.1	81
30	Microfluorescence and Microtomography Analyses of Heterogeneous Earth and Environmental Materials. Reviews in Mineralogy and Geochemistry, 2002, 49, 429-483.	4.8	79
31	Enhanced zinc consumption causes memory deficits and increased brain levels of zinc. Physiology and Behavior, 2005, 83, 793-803.	2.1	69
32	Redox state of Earth's magma ocean and its Venus-like early atmosphere. Science Advances, 2020, 6, .	10.3	69
33	Natural organobromine in marine sediments: New evidence of biogeochemical Br cycling. Global Biogeochemical Cycles, 2010, 24, .	4.9	65
34	The Role of CAX1 and CAX3 in Elemental Distribution and Abundance in Arabidopsis Seed Â. Plant Physiology, 2012, 158, 352-362.	4.8	64
35	Spatial and Temporal Variability of Arsenic Solid-State Speciation in Historically Lead Arsenate Contaminated Soils. Environmental Science & Technology, 2006, 40, 673-679.	10.0	63
36	Ancient water on asteroid 4 Vesta: evidence from a quartz veinlet in the Serra de Magé eucrite meteorite. Earth and Planetary Science Letters, 2004, 219, 189-199.	4.4	57

#	Article	IF	CITATIONS
37	A Mössbauer-based XANES calibration for hydrous basalt glasses reveals radiation-induced oxidation of Fe. American Mineralogist, 2018, 103, 489-501.	1.9	57
38	U-Pb dating of major and accessory minerals formed during metamorphism and deformation of metapelites. Geochimica Et Cosmochimica Acta, 1995, 59, 2513-2526.	3.9	56
39	Direct characterization of airborne particles associated with arsenic-rich mine tailings: Particle size, mineralogy and texture. Applied Geochemistry, 2011, 26, 1639-1648.	3.0	56
40	Getting to the core of platinum drug bio-distributions: the penetration of anti-cancer platinum complexes into spheroid tumour models. Metallomics, 2012, 4, 1209.	2.4	56
41	Assessment and control of organic and other contaminants associated with the Stardust sample return from comet 81P/Wild 2. Meteoritics and Planetary Science, 2010, 45, 406-433.	1.6	55
42	Chemical complexity induced local structural distortion in NiCoFeMnCr high-entropy alloy. Materials Research Letters, 2018, 6, 450-455.	8.7	54
43	Cerium Substitution in Yttrium Iron Garnet: Valence State, Structure, and Energetics. Chemistry of Materials, 2014, 26, 1133-1143.	6.7	53
44	Oxidizing Behavior of Soil Manganese. Soil Science Society of America Journal, 2005, 69, 87-95.	2.2	52
45	Synchrotron X-ray 2D and 3D elemental imaging of CdSe/ZnS quantum dot nanoparticles in Daphnia magna. Analytical and Bioanalytical Chemistry, 2009, 394, 911-917.	3.7	50
46	Crystallization conditions of Los Angeles, a basaltic Martian meteorite. Geochimica Et Cosmochimica Acta, 2002, 66, 1867-1880.	3.9	49
47	Soil Manganese Oxides and Trace Metals. Soil Science Society of America Journal, 2005, 69, 353-361.	2.2	49
48	Tropical dendrochemistry: A novel approach to estimate age and growth from ringless trees. Geophysical Research Letters, 2006, 33, .	4.0	48
49	Quantitative Determination of Absolute Organohalogen Concentrations in Environmental Samples by X-ray Absorption Spectroscopy. Analytical Chemistry, 2006, 78, 5711-5718.	6.5	45
50	U(<scp>v</scp>) in metal uranates: a combined experimental and theoretical study of MgUO ₄ , CrUO ₄ , and FeUO ₄ . Dalton Transactions, 2016, 45, 4622-4632.	3.3	45
51	Application of Synchrotron Xâ€Ray Microbeam Spectroscopy to the Determination of Metal Distribution and Speciation in Biological Tissues. Spectroscopy Letters, 2005, 38, 343-363.	1.0	44
52	Evidence for Biogenic Pyromorphite Formation by the NematodeCaenorhabditis elegans. Environmental Science & Technology, 2005, 39, 5620-5625.	10.0	42
53	Evaluating the cement stabilization of arsenic-bearing iron wastes from drinking water treatment. Journal of Hazardous Materials, 2015, 300, 522-529.	12.4	42
54	The bulk valence state of Fe and the origin of water in chondrites. Geochimica Et Cosmochimica Acta, 2017, 211, 115-132.	3.9	42

#	Article	IF	CITATIONS
55	Distribution of Chromium Contamination and Microbial Activity in Soil Aggregates. Journal of Environmental Quality, 2003, 32, 541-549.	2.0	41
56	Structure and thermodynamics of uranium-containing iron garnets. Geochimica Et Cosmochimica Acta, 2016, 189, 269-281.	3.9	41
57	Phosphor imaging as a tool for in situ mapping of ppm levels of uranium and thorium in rocks and minerals. Chemical Geology, 2003, 193, 127-136.	3.3	40
58	Zinc Coordination to Multiple Ligand Atoms in Organic-Rich Surface Soils. Environmental Science & Technology, 2006, 40, 5688-5695.	10.0	39
59	Spectroscopic Evidence of Uranium Immobilization in Acidic Wetlands by Natural Organic Matter and Plant Roots. Environmental Science & Technology, 2015, 49, 2823-2832.	10.0	39
60	Solubility and speciation of iron in hydrothermal fluids. Geochimica Et Cosmochimica Acta, 2019, 252, 126-143.	3.9	38
61	Retention and chemical speciation of uranium in an oxidized wetland sediment from the Savannah River Site. Journal of Environmental Radioactivity, 2014, 131, 40-46.	1.7	37
62	Shock-transformation of whitlockite to merrillite and the implications for meteoritic phosphate. Nature Communications, 2017, 8, 14667.	12.8	37
63	Real–Time Speciation of Uranium during Active Bioremediation and U(IV) Reoxidation. Journal of Environmental Engineering, ASCE, 2008, 134, 78-86.	1.4	36
64	Structural environment of iron and accurate determination of Fe3+/ΣFe ratios in andesitic glasses by XANES and Mössbauer spectroscopy. Chemical Geology, 2016, 428, 48-58.	3.3	36
65	Chemical composition and heterogeneity of Wild 2 cometary particles determined by synchrotron Xâ€ray fluorescence. Meteoritics and Planetary Science, 2008, 43, 187-213.	1.6	35
66	Redox systematics of martian magmas with implications for magnetite stability. American Mineralogist, 2013, 98, 616-628.	1.9	35
67	Substitution and diffusion of Cr2+ and Cr3+ in synthetic forsterite and natural olivine at 1200–1500â€ [–] °C and 1†bar. Geochimica Et Cosmochimica Acta, 2018, 220, 407-428.	3.9	35
68	Characterization of Petroleum Deposits Formed in a Producing Well by Synchrotron Radiation-Based Microanalyses. Energy & Fuels, 2004, 18, 1199-1212.	5.1	34
69	Sensitivity of Soil Manganese Oxides. Soil Science Society of America Journal, 2001, 65, 736-743.	2.2	33
70	Petrographic and trace element analysis of uranium-rich tufa calcite, middle Miocene Barstow Formation, California, USA. Sedimentology, 2004, 51, 433-453.	3.1	33
71	Redox evolution of silicic magmas: Insights from XANES measurements of Ce valence in Bishop Tuff zircons. Chemical Geology, 2015, 402, 77-88.	3.3	33
72	Hyperspectral image reconstruction for x-ray fluorescence tomography. Optics Express, 2015, 23, 9014.	3.4	33

5

#	Article	IF	CITATIONS
73	Geochemical Signature of Contaminated Sediment Remobilization Revealed by Spatially Resolved X-ray Microanalysis of Annual Rings of Salix nigra. Environmental Science & Technology, 2003, 37, 1766-1774.	10.0	32
74	Gadolinium deposition in nephrogenic systemic fibrosis: An examination of tissue using synchrotron x-ray fluorescence spectroscopy. Journal of the American Academy of Dermatology, 2010, 62, 38-44.	1.2	32
75	Accurate determination of ferric iron in garnets by bulk Mossbauer spectroscopy and synchrotron micro-XANES. American Mineralogist, 2012, 97, 1726-1740.	1.9	31
76	Distribution and Speciation of Metals in Annual Rings of Black Willow. Journal of Environmental Quality, 2005, 34, 1165-1173.	2.0	30
77	Thickness measurements of nanoscale brine films on silica surfaces under geologic CO ₂ sequestration conditions using synchrotron Xâ€ray fluorescence. Water Resources Research, 2012, 48, .	4.2	30
78	Use of multivariate analysis for synchrotron micro-XANES analysis of iron valence state in amphiboles. American Mineralogist, 2016, 101, 1171-1189.	1.9	30
79	Charge-Coupled Substituted Garnets (Y _{3–<i>x</i>} Ca _{0.5<i>x</i>} M _{0.5<i>x</i>})Fe ₅ O _{12(M = Ce, Th): Structure and Stability as Crystalline Nuclear Waste Forms. Inorganic Chemistry, 2015, 54, 4156-4166.}	ub> 4.0	29
80	Evaluating zinc isotope fractionation under sulfate reducing conditions using a flow-through cell and in situ XAS analysis. Geochimica Et Cosmochimica Acta, 2017, 203, 1-14.	3.9	29
81	An assessment of the utility of staurolite in U-Pb dating of metamorphism. Contributions To Mineralogy and Petrology, 1997, 129, 352-365.	3.1	27
82	8. Microfluorescence and Microtomography Analyses of Heterogeneous Earth and Environmental Materials. , 2002, , 429-484.		26
83	Scanning X-ray Fluorescence Imaging Study of Lithium Insertion into Copper Based Oxysulfides for Li-Ion Batteries. Chemistry of Materials, 2012, 24, 2684-2691.	6.7	26
84	Accurate predictions of iron redox state in silicate glasses: A multivariate approach using X-ray absorption spectroscopy. American Mineralogist, 2016, 101, 744-747.	1.9	26
85	Sensitivity of Soil Manganese Oxides. Soil Science Society of America Journal, 2001, 65, 744-752.	2.2	25
86	X27A—A new hard X-ray micro-spectroscopy facility at the National Synchrotron Light Source. Nuclear Instruments and Methods in Physics Research, Section A: Accelerators, Spectrometers, Detectors and Associated Equipment, 2006, 562, 487-494.	1.6	25
87	Long-Term Stability of Organic Carbon-Stimulated Chromate Reduction in Contaminated Soils and Its Relation to Manganese Redox Status. Environmental Science & Technology, 2007, 41, 4326-4331.	10.0	25
88	Assessing heavy metal exposure in Renaissance Europe using synchrotron microbeam techniques. Journal of Archaeological Science, 2014, 52, 204-217.	2.4	25
89	Spatially Resolved Elemental Analysis, Spectroscopy and Diffraction at the GSECARS Sector at the Advanced Photon Source. Journal of Environmental Quality, 2017, 46, 1158-1165.	2.0	24
90	Ion Diffusion Within Water Films in Unsaturated Porous Media. Environmental Science & Technology, 2017, 51, 4338-4346.	10.0	24

#	Article	IF	CITATIONS
91	Use of the spindle stage for orientation of single crystals for microXAS: Isotropy and anisotropy in Fe-XANES spectra. American Mineralogist, 2002, 87, 1500-1504.	1.9	23
92	The effect of ore roasting on arsenic oxidation state and solid phase speciation in gold mine tailings. Geochemistry: Exploration, Environment, Analysis, 2015, 15, 273-291.	0.9	23
93	Depositional and diagenetic constraints on the abundance and spatial variability of carbonate-associated sulfate. Chemical Geology, 2019, 523, 59-72.	3.3	23
94	Uranium Reduction in Sediments under Diffusion-Limited Transport of Organic Carbon. Environmental Science & Technology, 2005, 39, 7077-7083.	10.0	22
95	Titanium and Iron in Lung of a Soldier With Nonspecific Interstitial Pneumonitis and Bronchiolitis After Returning From Iraq. Journal of Occupational and Environmental Medicine, 2012, 54, 1-2.	1.7	22
96	Real-Time X-ray Absorption Spectroscopy of Uranium, Iron, and Manganese in Contaminated Sediments During Bioreduction. Environmental Science & Technology, 2008, 42, 2839-2844.	10.0	21
97	Characterization of heterogeneities in detector-grade CdZnTe crystals. Journal of Materials Research, 2009, 24, 1361-1367.	2.6	21
98	SMART mineral mapping: Synchrotron-based machine learning approach for 2D characterization with coupled micro XRF-XRD. Computers and Geosciences, 2021, 156, 104898.	4.2	19
99	241Am, 137Cs, Sr and Pb uptake by tobacco as influenced by application of Fe chelators to soil. Journal of Environmental Radioactivity, 2005, 82, 33-50.	1.7	18
100	Characterization of geosynthetic clay liner bentonite using micro-analytical methods. Applied Geochemistry, 2010, 25, 1056-1069.	3.0	18
101	Tools for uranium characterization in carbonate samples: case studies of natural U–Pb geochronology reference materials. Geochronology, 2021, 3, 103-122.	2.5	18
102	Trends in X-ray Fluorescence Microscopy. Synchrotron Radiation News, 2013, 26, 32-38.	0.8	17
103	Heavy metal distribution in an urban wetland impacted by combined sewer overflow. Chemosphere, 2013, 93, 2159-2164.	8.2	17
104	In situ measurement of ferric iron in lunar glass beads using Fe-XAS. Icarus, 2017, 285, 95-102.	2.5	16
105	Accurate predictions of microscale oxygen barometry in basaltic glasses using V K-edge X-ray absorption spectroscopy: A multivariate approach. American Mineralogist, 2018, 103, 1282-1297.	1.9	16
106	Vanadium, sulfur, and iron valences in melt inclusions as a window into magmatic processes: A case study at Nyamuragira volcano, Africa. Geochimica Et Cosmochimica Acta, 2018, 226, 149-173.	3.9	15
107	Direct measurements of copper speciation in basaltic glasses: understanding the relative roles of sulfur and oxygen in copper complexation in melts. Geochimica Et Cosmochimica Acta, 2019, 267, 164-178.	3.9	15
108	Oxybarometry and valence quantification based on microscale X-ray absorption fine structure (XAFS) spectroscopy of multivalent elements. Chemical Geology, 2020, 531, 119305.	3.3	15

#	Article	IF	CITATIONS
109	Synchrotron X-ray microprobe and computed microtomography for characterization of nanocatalysts. Nuclear Instruments & Methods in Physics Research B, 2005, 241, 331-334.	1.4	14
110	Identification and Characterization of Arsenic and Metal Compounds in Contaminated Soil, Mine Tailings, and House Dust Using Synchrotron-Based Microanalysis. Human and Ecological Risk Assessment (HERA), 2011, 17, 1292-1309.	3.4	14
111	Copper complexation and solubility in high-temperature hydrothermal fluids: A combined study by Raman, X-ray fluorescence, and X-ray absorption spectroscopies and ab initio molecular dynamics simulations. Chemical Geology, 2018, 494, 69-79.	3.3	14
112	Improving the reliability of Fe- and S-XANES measurements in silicate glasses: Correcting beam damage and identifying Fe-oxide nanolites in hydrous and anhydrous melt inclusions. Chemical Geology, 2021, 586, 120610.	3.3	14
113	Synchrotron Xâ€ray fluorescence spectroscopy of salts in natural sea ice. Earth and Space Science, 2016, 3, 463-479.	2.6	13
114	Five Hundred Years of Mercury Exposure and Adaptation. Journal of Biomedicine and Biotechnology, 2012, 2012, 1-10.	3.0	12
115	Insights into past ocean proxies from micron-scale mapping of sulfur species in carbonates. Geology, 2019, 47, 833-837.	4.4	12
116	Localization of Free and Bound Metal Species through X-Ray Synchrotron Fluorescence Microscopy in the Rodent Brain and Their Relation to Behavior. Brain Sciences, 2019, 9, 74.	2.3	12
117	Variation in XANES in biotite as a function of orientation, crystal composition, and metamorphic history. American Mineralogist, 2014, 99, 443-457.	1.9	11
118	Intraplate mantle oxidation by volatile-rich silicic magmas. Lithos, 2017, 292-293, 320-333.	1.4	11
119	Characterization of carbon―and nitrogenâ€rich particle fragments captured from comet 81P/Wild 2. Meteoritics and Planetary Science, 2008, 43, 335-351.	1.6	10
120	The source of sulfate in brachiopod calcite: Insights from μ-XRF imaging and XANES spectroscopy. Chemical Geology, 2019, 529, 119328.	3.3	10
121	Cation Exchange in Smectites as a New Approach to Mineral Carbonation. Frontiers in Climate, 0, 4, .	2.8	9
122	Distribution of Chromium Contamination and Microbial Activity in Soil Aggregates. Journal of Environmental Quality, 2003, 32, 541.	2.0	8
123	Sulfides from martian and lunar basalts: Comparative chemistry for Ni, Co, Cu, and Se. American Mineralogist, 2011, 96, 932-935.	1.9	8
124	The sub-micron resolution X-ray spectroscopy beamline at NSLS-II. Nuclear Instruments and Methods in Physics Research, Section A: Accelerators, Spectrometers, Detectors and Associated Equipment, 2011, 649, 46-48.	1.6	8
125	Quantifying and correcting the effects of anisotropy in XANES measurements of chromium valence in olivine: Implications for a new olivine oxybarometer. American Mineralogist, 2017, 102, 1165-1172.	1.9	8
126	Practical Application of Synchrotron-Based Hard X-Ray Microprobes in Soil Sciences. Developments in Soil Science, 2010, 34, 27-72.	0.5	7

#	Article	IF	CITATIONS
127	Enhanced Immobilization of Arsenic from Acid Mine Drainage by Detrital Clay Minerals. ACS Earth and Space Chemistry, 2019, 3, 2525-2538.	2.7	7
128	Constraints on timing and displacement of multistage shearing in the Norumbega fault system, eastern Maine. , 1999, , .		6
129	Development and applications of an epifluorescence module for synchrotron x-ray fluorescence microprobe imaging. Review of Scientific Instruments, 2005, 76, 066107.	1.3	6
130	Effect of Saline Waste Solution Infiltration Rates on Uranium Retention and Spatial Distribution in Hanford Sediments. Environmental Science & amp; Technology, 2008, 42, 1973-1978.	10.0	6
131	Differences in Fe-redox for asbestiform and nonasbestiform amphiboles from the former vermiculite mine, near Libby, Montana, U.S.A American Mineralogist, 2011, 96, 1414-1417.	1.9	6
132	Structure and thermodynamic stability of UTa ₃ O ₁₀ , a U(<scp>v</scp>)-bearing compound. Dalton Transactions, 2016, 45, 18892-18899.	3.3	6
133	In-situ mapping of ferric iron variations in lunar glasses using X-ray absorption spectroscopy. American Mineralogist, 2019, 104, 453-458.	1.9	6
134	A synchrotron-based facility for the in-situ location, chemical and mineralogical characterization of â^¼10μm particles captured in aerogel. Advances in Space Research, 2009, 43, 328-334.	2.6	5
135	Biologic Rhythms Derived from Siberian Mammoths' Hairs. PLoS ONE, 2011, 6, e21705.	2.5	5
136	Oxidation of Added Mn(II) in Soils Observed by XANES Spectroscopy and Cr(III) Oxidation. Soil Science Society of America Journal, 2013, 77, 1996-2003.	2.2	5
137	The absorption indicatrix as an empirical model to describe anisotropy in X-ray absorption spectra of pyroxenes. American Mineralogist, 2022, 107, 654-663.	1.9	5
138	Rapid reduction of basaltic glasses in piston-cylinder experiments: a XANES study. Contributions To Mineralogy and Petrology, 2021, 176, 1.	3.1	4
139	Imaging and microspectroscopy at the national synchrotron light source. Synchrotron Radiation News, 2002, 15, 17-26.	0.8	3
140	An Experimental-XANES Investigation of Cr Valence Systematics in Basaltic Liquids and Applications to Modeling Cr2+/ Σ Cr Evolution in Crystallizing Basaltic Magma Systems. Geochimica Et Cosmochimica Acta, 2021, 292, 130-151.	3.9	3
141	High-speed, coupled micro-beam XRD/XRF/XAFS mapping at GSECARS: APS Beamline 13-ID-E. , 2016, , 53-64.		3
142	Accessing User Facilities and Making Your Research Experience Successful. Elements, 2006, 2, 31-35.	0.5	2
143	Using the NSLS for Introducing Synchrotrons into the Classroom (InSynC). Synchrotron Radiation News, 2013, 26, 30-34.	0.8	2
144	Focus on Synchrotron Education Initiatives. Synchrotron Radiation News, 2013, 26, 2-4.	0.8	2

#	Article	IF	CITATIONS
145	Trace elemental behavior in the solar nebula: Synchrotron X-ray fluorescence analyses of CM and CR chondritic iron sulfides and associated metal. Geochimica Et Cosmochimica Acta, 2021, 310, 131-154.	3.9	2
146	Synchrotron-based imaging detects metal and plaques in a mouse model of Alzheimer's Disease. , 2007, , .		1
147	Technical Report: Growth of Environmental Science at the NSLS. Synchrotron Radiation News, 2007, 20, 6-13.	0.8	1
148	Macroscopic and molecular-scale assessment of soil lead contamination impacted by seasonal dove hunting activities. Journal of Soils and Sediments, 2011, 11, 968-979.	3.0	1
149	Selective Ion Accumulation in Biomineralizing Marine Acantharia. Microscopy and Microanalysis, 2019, 25, 1072-1073.	0.4	1
150	Radiation-Induced Changes in Vanadium Speciation in Basaltic Glasses: Implications for Oxybarometry Measurements Using Vanadium K-edge X-ray Absorption Spectroscopy. American Mineralogist, 2021, , .	1.9	1
151	Valence determinations and oxybarometry on FIBâ€sectioned olivine and pyroxene using correlated Ti, V, and Cr microâ€XAFS spectroscopy: Evaluation of ionâ€milling effects and application to Antarctic micrometeorite grains. Meteoritics and Planetary Science, 2020, 55, 2553-2569.	1.6	1
152	Synchrotron radiation needs for molecular environmental science. Eos, 2007, 88, 571-571.	0.1	0
153	Energy, Enthusiasm, Cooperation, and Commitment Characterize NUFO Annual Meeting. Synchrotron Radiation News, 2011, 24, 13-14.	0.8	Ο
154	Neurotoxins during the Renaissance. Bioarcheology of Ferrante II of Aragon (1469–1496) and Isabella of Aragon (1470–1524). Journal of Archaeological Science: Reports, 2016, 5, 542-546.	0.5	0
155	<i>IN SITU </i> MEASUREMENT OF FERRIC IRON IN LUNAR GLASS BEADS USING FE-XAS. , 2016, , .		Ο
156	HIGH ENERGY SYNCHROTRON X-RAY MICROSPECTROSCOPY FOR GEOCHEMICAL CHARACTERIZATION OF TERRESTRIAL AND EXTRATERRESTRIAL SAMPLES. , 2016, , .		0
157	INVESTIGATIONS INTO THE DEGASSING OF NYAMURAGIRA VOLCANO (D.R. CONGO, AFRICA) THROUGH SYNCHROTRON MICRO-XANES ANALYSIS. , 2016, , .		Ο
158	ARSENIC REMOVAL FROM HIGH SALINITY WASTEWATER THROUGH BARITE CO-PRECIPITATION. , 2017, , .		0